Frequency Tunable, Cavity-Enhanced Single Erbium Quantum Emitter in the Telecom Band

Yu, Yong; Oser, Dorian; Da Prato, Gaia; Urbinati, Emanuele; Ávila, Javier Carrasco; Zhang, Yu; Remy, Patrick; Marzban, Sara; Gröblacher, Simon; Tittel, Wolfgang

Important note
To cite this publication, please use the final published version (if applicable).
Please check the document version above.

Frequency Tunable, Cavity-Enhanced Single Erbium Quantum Emitter in the Telecom Band

Yong Yu[,1] Dorian Oser[,2,*] Gaia Da Prato[,1] Emanuele Urbinati[,1] Javier Carrasco Ávila[,3,4] Yu Zhang[,1]
Patrick Remy[,5] Sara Marzban[,2,†] Simon Gröblacher[,1,‡] and Wolfgang Tittel[2,3,4,§]

[1]*Kavli Institute of Nanoscience, Department of Quantum Nanoscience,*
Delft University of Technology, 2628CJ Delft, The Netherlands
[2]*QuTech, Delft University of Technology, 2628CJ Delft, The Netherlands*
[3]*Department of Applied Physics, University of Geneva, 1211 Geneva, Switzerland*
[4]*Constructor University Bremen, 28759 Bremen, Germany*
[5]*SIMH Consulting, Rue de Genève 18, 1225 Chêne-Bourg, Switzerland*

Single quantum emitters embedded in solid-state hosts are an ideal platform for realizing quantum information processors and quantum network nodes. Among the currently investigated candidates, Er^{3+} ions are particularly appealing due to their 1.5 µm optical transition in the telecom band as well as their long spin coherence times. However, the long lifetimes of the excited state—generally in excess of 1 ms—along with the inhomogeneous broadening of the optical transition result in significant challenges. Photon emission rates are prohibitively small, and different emitters generally create photons with distinct spectra, thereby preventing multiphoton interference—a requirement for building large-scale, multinode quantum networks. Here we solve this challenge by demonstrating for the first time linear Stark tuning of the emission frequency of a single Er^{3+} ion. Our ions are embedded in a lithium niobate crystal and couple evanescently to a silicon nanophotonic crystal cavity that provides a strong increase of the measured decay rate. By applying an electric field along the crystal c axis, we achieve a Stark tuning greater than the ion's linewidth without changing the single-photon emission statistics of the ion. These results are a key step towards rare earth ion-based quantum networks.

Quantum emitters play a vital role in future quantum networks [1,2]. They serve as the crucial light-matter interface, bridging static qubits that handle local quantum information processing with flying qubits, which are responsible for remote information transfer. Compared with quantum emitter platforms such as trapped neutral atoms [3,4], ions [5], and quantum dots [6], single defects in the solid state [7] have proven to be among the most successful, owing to their ease of use and potential for large-scale integration. Notably, defects such as nitrogen-vacancy and silicon-vacancy centers in diamond [8] have recently been used for seminal demonstrations of multi-node quantum networks [9,10] and memory-enhanced quantum communication [11], respectively. One major downside for these defects is that they operate at visible or close-to-visible optical wavelengths and are therefore subject to significant transmission loss that exceeds 2 dB/km of fiber, which hampers their integration into large-scale quantum networks [12]. In addition, their optical coherence time is typically limited to a few tens of nanoseconds, restricting their suitability for ensemble-based quantum memory for light [13].

Trivalent rare-earth ions (REIs) represent another type of solid-state defect [14]. Their $4f$ electrons are effectively shielded by filled outer electronic shells, resulting in narrow linewidths—or long coherence times—for $4f - 4f$ transitions in the optical band and spin-state transitions in the microwave regime. This makes them ideally suited as ensemble-based optical quantum memories [15] with high efficiency [16–18], long storage times [13,19,20], large bandwidth [21], high fidelity [22], and large multimode capacity [23]. Using individual REIs (instead of ensembles) furthermore allows the creation of true single photons [24–32] and promises quantum information processing with qubits encoded into spin states [33] that can feature coherence times up to a few hours [34]. This large versatility sets rare-earth-doped crystals apart from any other solid-state impurity.

However, using individual REIs—either for sources or for qubits—is challenging because of their long excited-state lifetimes and hence low photon emission rate. The most practical way to overcome this problem is to Purcell enhance [4] a spectrally isolated ion within the inhomogeneously broadened transition. By fabricating a nanoscale photonic-crystal (PhC) cavity out of the rare-earth-doped crystal [26,29,30] or by bringing a separately fabricated PhC cavity in close proximity to the REI-doped material [25], ion emission within the cavity mode is strongly

enhanced. Using this approach, single-photon sources and nondemolition measurements have been demonstrated [27–31]. The enhanced interaction with light also enables coupling between a single REI and neighboring nuclear spins [35,36], and, in future, between neighboring REIs [33] as well as photon-mediated entangling of distant REIs [37].

Unfortunately, the spectral properties of the emitted photons are largely determined by their local environment, leading to distinguishable spectral lines and spectral diffusion [14]. While a quantum eraser technique [38] allows
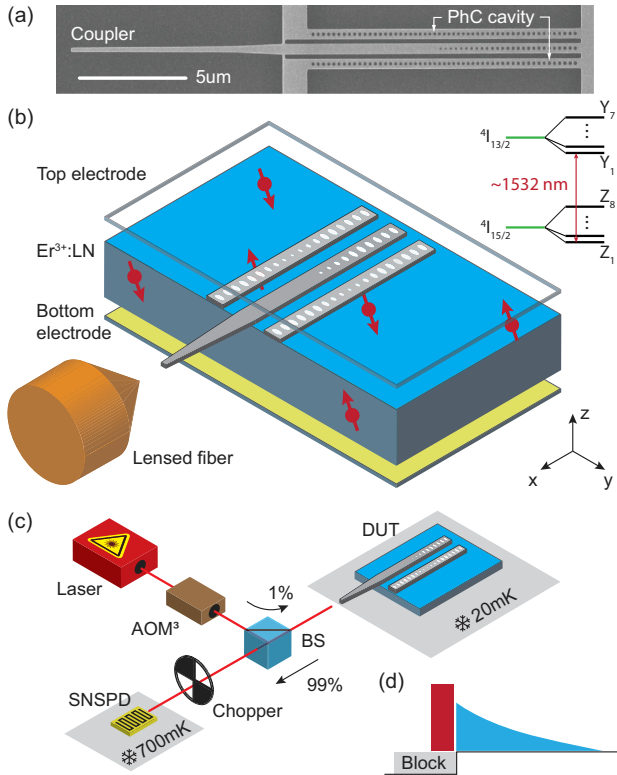

FIG. 1. Experimental setup. (a) A scanning electron microscopic image of the PIC, consisting of two PhC cavities and a tapered waveguide in the middle as a common coupler. (b) Schematic of the device. The silicon PIC is placed on an Er:LN crystal and is optically accessed via a lensed fiber. A pair of electrodes above and below the LN crystal allows applying an electric field. The top right inset shows a simplified energy level scheme of Er:LN at no magnetic field. The crystal field splits the $^{2S+1}L_J$ states of the free Er^{3+} ion (green lines) into $J + 1/2$ Kramers doublets (black lines). The $Z_1 - Y_1$ transition is at around 1532 nm. (c) Optical setup for measuring PL. Three concatenated acoustic optical modulators (AOMs) are used to create excitation pulses from a continuous wave laser. A 99∶1 beam splitter (BS) routes the excitation pulse to the DUT and guides the light emitted from the sample to the detection setup. After an optical chopper, which blocks the reflected excitation pulses, a SNSPD detects the PL signal. (d) Time sequence of the experiment. The exponentially decaying PL (blue) is collected after a short excitation pulse (red) is sent.

entangling photons with a frequency difference of ∼80 MHz (and potentially up to a few Gigahertz using high-bandwidth detectors), it is generally preferable to use indistinguishable photons for this operation, which is crucial in quantum networks. As a consequence, two-photon interference of the Hong-Ou-Mandel type has so far merely been demonstrated between two consecutive photons from the same REI emitter [31], embedded inside a specific host crystal that limits spectral diffusion but, at the same time, also prevents external spectral control.

In this Letter, we demonstrate for the first time spectral engineering of a single cavity-enhanced REI emitter. We choose erbium ion (Er^{3+}), which is particularly attractive as its telecom C-band optical transition provides an opportunity to directly access fiber-based networks with minimal loss. More precisely, we use evanescently coupled silicon nanophotonic cavities to Purcell-enhance and collect the emission from Er^{3+} doped into a lithium niobate crystal. We observe an up to 143-fold increase in the decay rate of the excited state (i.e., a reduction of the lifetime T_1 from 1.8 ms to 12.5 μs) and, for ions with Purcell factors up to 13, we measure autocorrelation coefficients of the emitted light around 0.2, indicating single ions [39]. We then control the ion frequency by applying an electric field along the z axis of the $LiNbO_3$ (LN) crystal. This allows us to demonstrate a frequency tunability greater than the emitter linewidth (measured during around 1 min) without compromising the single-quantum character of the emitter. This promises making different emitters spectrally indistinguishable and countering spectral diffusion through feedback [40]. Our findings complement those in Ref. [29], in which an electric field was used to tune the cavity resonance but not that of the Er^{3+} ions.

The experimental device utilized in this study is comprised of a z-cut LN crystal doped with 50 ppm of erbium ions and a photonic integrated chip (PIC) containing two nanofabricated silicon PhC cavities and a common coupler waveguide, nearly critically coupled to both PhC cavities [see Figs. 1(a) and 1(b)]. We fabricate the PICs separately from a silicon-on-insulator wafer with a 250 nm device layer and transfer it to the surface of the LN crystal using a pick-and-place technique [41]. LN is chosen because of its inversionless site symmetry, which allows linear Stark tuning of the Er^{3+} ions' transition frequency [42,43]. The symmetry furthermore determines the transition dipoles to be oriented along the x-y plane of the crystal. Ions near the LN surface therefore couple evanescently to the transverse electric (TE) field of the cavity. The PhC cavities on the LN substrate have a typical quality factor of $Q = 50\,000$, and finite-element simulations reveal mode volumes of 0.09 μm³ and an evanescent field strength at the Si-LN interface around 45% of its maximal value. Additionally considering the branching ration of 0.22 [44], this leads to a maximal enhancement of the Y_1 to Z_1 emission rate of 220. The device under test (DUT) is
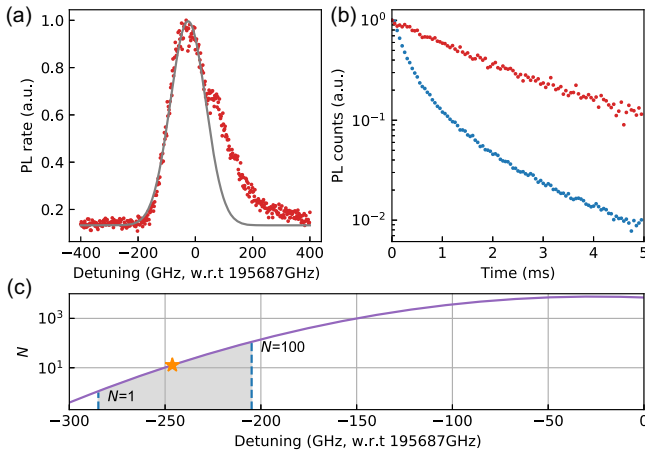
FIG. 2.   Characterization of ensemble Er^{3+} ions. (a) PL spectrum of the Er^{3+} ions under the coupler waveguide. The gray curve shows a Gaussian fit. (b) Time-resolved PL of ions with PhC cavity enhancement (blue, cavity resonance at 1532.5 nm) and without enhancement (red). (c) Simulated average cavity-addressable ion number N within a frequency interval of 4 GHz as a function of the cavity resonance frequency. The star marks the frequency used in the single-ion measurements. The gray shaded area indicates the frequency region where spectrally resolved single ions are expected, with two blue dashed lines identifying $N = 1$ and 100.

furthermore equipped with two parallel copper electrodes positioned above and below the 2 mm thick sample, which allows the creation of an electric field along the crystal z direction. The coupler waveguide end is inverse tapered and sticks out of the LN sample. Light is coupled from and to a lensed fiber with typical fiber coupling efficiencies of around 60%. The whole device is cooled inside a dilution refrigerator to around 20 mK [45].

In a first step we characterize ensemble properties of Er:LN, starting with its inhomogeneously broadened absorption line. Towards this end we employ photoluminescence (PL) excitation spectroscopy with the setup and the time sequence shown in Figs. 1(c) and 1(d), respectively. We excite ions near the Si-LN interface with a short optical pulse (∼1 μs) and record their emission using a superconducting nanowire single photon detector (SNSPD). We choose a cavity with a resonance far away from the Er^{3+} transition such that ions solely couple to the coupler waveguide. By scanning the excitation laser frequency around the $Z_1 − Y_1$ transition of Er^{3+} at around 1532 nm, we obtain the spectrum shown in Fig. 2(a). Neglecting the bulge arising from a phonon sideband transition [45], we extract a Gaussian inhomogeneous line centered at 1531.8 nm with 145.3 GHz width, in good agreement with the literature value [46]. Combining the knowledge of the Er^{3+} frequency distribution with the ion density and cavity mode distribution, we calculate the average ion number N within the PhC cavity linewidth as a function of the cavity resonance frequency [45]. In order to
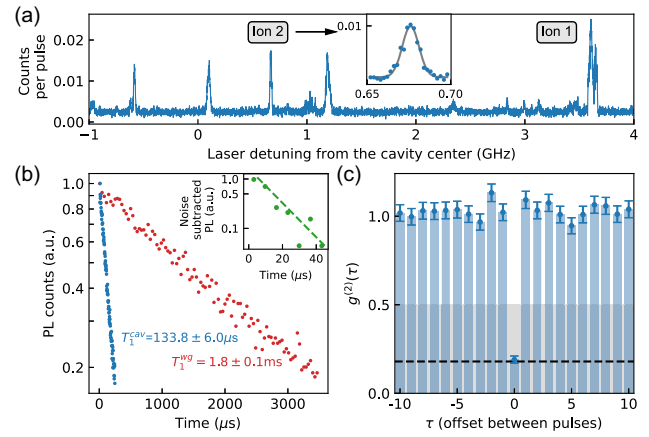
FIG. 3.   Characterization of Er^{3+} ions in the few- or single-ion regime. (a) PL spectrum of ions coupled to a PhC cavity. The spectrum is measured with 1 MHz precision and each data point is accumulated for 6 s. The inset shows an enlarged spectrum of the PL peak labeled ion 2 (blue dots) and a Gaussian fit (gray line) with 11.1 MHz FWHM. The units of the axes are as in the main figure. (b) Time-resolved photon emission from the cavity-enhanced PL line "ion 1" (blue). The PL decay of the Er^{3+} ensemble that couples only to the waveguide is shown for comparison (red). The inset shows the decay using another PhC cavity with a decay constant of 12.5 ± 3.9 μs [$g^{(2)}(\tau)$ not measured for noisy data [45]]. (c) Second-order auto-correlation function $g^{(2)}(\tau)$ measured during 30 min with photons from PL line "ion" 1 using a Hanbury Brown–Twiss setup. We group all photon detections during 90 μs after each excitation pulse into a single time bin, and the horizontal axis shows the autocorrelation coefficient as a function of the difference between excitation pulses. The error bars represent one standard deviation. The gray shaded area indicates the single emitter regime and the black dashed line shows the dark count contribution.

spectrally resolve single ions within the cavity, one needs an average ion number per mode volume and resonance width between 1 and 100. The total frequency range for this is ∼80 GHz, as indicated in Fig. 2(c).

Next, we pick a PhC cavity with resonance centered on the inhomogeneous line, which allows us to observe cavity-based enhancement of the ensemble decay rate [Fig. 2(b)]. The PL signal shows a 250 times larger intensity and a significantly decreased decay time. The nonexponential decay profile is caused by contributions from different ions that experience different magnitudes of enhancement [54].

As the second step, we look for spectrally isolated ions coupled to a PhC cavity. Towards this end, we choose a cavity with resonance within the tail of the inhomogeneously broadened Er^{3+} line to reduce the average number of ions within the cavity linewidth. Specifically, we pick a wavelength of 1533.8952 nm [linewidth of 3.8 GHz, marked using a star in Fig. 2(c)]. Figure 3(a) depicts five individual PL peaks within the cavity linewidth, which we interpret as spectrally isolated single ions. Some of the less prominent peaks in the spectrum may be a result of ions

with reduced Purcell enhancement. We focus on the peak labeled Ion 1 in Fig. 3(a) for its brightness, and measure its time-resolved PL as shown in Fig. 3(b). We extract an exponential decay lifetime of 133.8 µs, 13-fold shorter than the waveguide measurement result. Measurements of additional PL peaks using another—except for the resonance frequency identical—PhC cavity [45] resulted in lifetimes as short as 12.5 µs [see inset of Fig. 3(b) and [45]], corresponding to rate enhancements up to a factor of 143. This is smaller than the expected value of 220, which we attribute to the nonideal positioning of the ions in the cavity field. Better-positioned ions may have been found by gas tuning the cavity [25].

To confirm that the individual PL lines arise from single emmiters, we measure the second-order auto-correlation coefficient $g^{(2)}(0)$ of the PL signal labeled ion 1. Its value of 0.19 ± 0.02, extracted from Fig. 3(c), is significantly lower than the threshold of 0.5 for two emitters [39], indicating that the majority of the detected photons stem from a single ion. We obtain similar results for other isolated PL lines, including the one labeled ion 2 in Fig. 3(a). Our analysis suggests that accidental coincidences between detected photons and dark counts fully account for the imperfect $g^{(2)}(0)$ [45]. To further improve the single-photon purity towards $g^{(2)}(0) = 0$, a higher signal-to-noise ratio is therefore required. This can be achieved by increasing the Purcell factor, which will improve the photon emission rate, and by optimizing the system efficiency.

We now tune the frequency of the Er^{3+} ions by applying an external dc electric field to the electrodes. This shifts the energy levels of emitters with a permanent dipole moment, known as the linear dc Stark effect [42]. When the dipole moments of the ground and of the excited states experience different shifts, the external electric field leads to a shift of the associated optical transition frequency. We focus on ion 2 (for its reduced spectral width compared to ion 1) and observe its frequency shift while cycling the voltage from 0 to 640 V multiple times in a linear fashion. The results are depicted in Fig. 4. We extract a Stark coefficient of 182.9 kHz/V mm^{-1}, not far from the literature value of 250 kHz/V mm^{-1} [43]. We attribute the small discrepancy to imperfect modeling of the electric field.

To confirm that the single-ion nature is not affected by the electric field, we furthermore measure the auto-correlation function under different electric field amplitudes. As shown in Fig. 4(b), $g^{(2)}(0)$ remains constant, close to the noise-limited threshold. This establishes Stark tuning as a useful tool for controlling the frequency of single rare-earth ions in quantum applications.

Finally, we give a brief outlook on the possibility of creating emitters in different crystals that emit indistinguishable photons. This implies (i) lifetime-limited, and (ii) identical spectra. Figure 3(a) shows that the measured linewidths of the observed PL peaks can be as small as 11 MHz, largely exceeding, e.g., the Fourier limit $\Delta\nu_F$ of
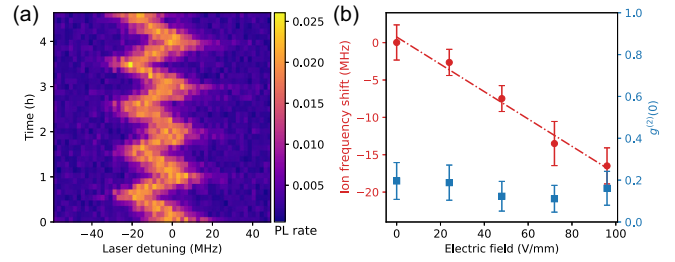

FIG. 4. Linear Stark tuning of a single Er^{3+} ion. (a) The spectral line of a single Er^{3+} ion shifts back and forth when a triangular voltage ramp is applied across the Er:LN crystal. (b) Frequency shift and autocorrelation coefficient $g^{(2)}(0)$ of emitted photons as a function of the electric field amplitude. The red dashed line is a linear fit to the frequency shift of the ion; error bars are calculated from data taken during different ramps. The error of the correlation coefficient is calculated from Poissonian photon counting statistics.

around 25 kHz imposed by the (reduced) lifetime of 12.5 µs ($\Delta\nu_F = 1/\pi T_1$). We attribute this excess broadening to measurement imperfections, including laser instability and power broadening that can be eliminated using an improved experimental setup [45], and spectral diffusion induced by spin flips and flip flops [46]. Polarizing the spin reservoir using a strong magnetic field or by lowering the temperature will provide a quieter local environment, thus reducing spectral diffusion [46].

For more insight, we "burn" spectral holes into the inhomogeneously broadened absorption line of an identical Er:LN bulk crystal, i.e., we reduce absorption within a narrow spectral interval through frequency-selective optical pumping with a coherent laser [47,48]. At a temperature of 1.1 K we observe the spectral hole width Γ_{hole}—which is directly related to the width of a PL peak—at different magnetic fields [45]. We find that Γ_{hole} (measured 380 µs after burning) decreases from ~3 MHz at a magnetic field of $B = 0$ T to 130 kHz at 1 T (Fig. 5). Significant additional narrowing is expected at a higher magnetic field and at a temperature of a few tens of mK [46], where coherence times up to 180 µs (equivalent to $\Gamma_{\text{hole}} \approx 3.5$ kHz) have been measured using two-pulse photon echoes (2PPE) [49]. (But note that 2PPE measurements happen on a shorter timescale than hole burning and are less affected by spectral diffusion.) We furthermore stress that the lifetime of the single emitter can be further decreased (and hence the related spectral width increased) by choosing an ion at an optimized location where the electric field is maximum, by decreasing the mode volume of the cavity, or by increasing its quality factor Q. We are therefore confident that, under readily achievable experimental conditions, the linewidth of an isolated PL peak becomes lifetime limited [45]. Additional spectral diffusion can be compensated using Stark-shift-based feedback, similar to what has been demonstrated with quantum dots using electric fields [40].
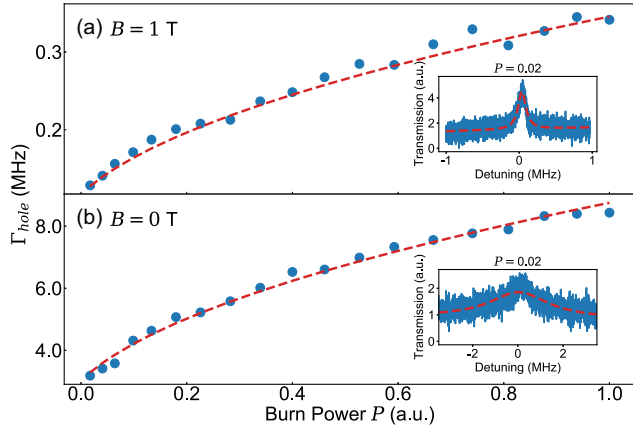
FIG. 5. (a) A spectral hole of 130 kHz width "burned" with minimum power into the inhomogeneously-broadened absorption line of Er:LN at $T = 1.1$ K and $B = 1$ T (inset), and hole widths Γ_{hole} as a function of burning power (main graph). For comparison, panel (b) shows a 3.2 MHz-wide hole created under the same conditions but at $B = 0$ T. Extrapolating the data in the main graphs to zero burning power, we find power broadening-free hole widths of 122 ± 4 kHz and 3.02 ± 0.10 MHz. Error bars are smaller than each data point.

Such Stark tuning also allows matching the spectra of two ions that are located in different crystals, thereby creating indistinguishable photons and enabling multiphoton interference. Because of the simple design of the electrodes in our proof-of-principle demonstration, the observed Stark shift is only slightly larger than the width of the ion's spectral line. However, much larger Stark tuning, up to gigahertz using only 20 V, can be expected by introducing nanoscale on-chip electrodes, for which the fabrication process is well developed and directly compatible with our fabrication process [29].

In summary, we have detected single photons from individual erbium ions using Purcell enhancement through a photonic crystal cavity. Additionally, we have demonstrated linear Stark tuning of the ion frequency without altering its single-photon emission statistics. By exploiting the piezo-optic effect of lithium niobate, it is furthermore possible to tune the cavity resonance, making Er:LN a versatile quantum emitter platform. However, to achieve lifetime-limited linewidth, a quieter spin bath and a more stable charge environment are required. The former can be created through low-dose ion implantation and by polarizing the spin bath using a large magnetic field or reducing the temperature, while the latter can be achieved by implementing Stark tuning-based feedback. This will allow dynamical compensation of spectral diffusion as well as spectral tunability, and thereby open the door to rare-earth-ion-based quantum networks.

Note added.—Recently, we became aware of the work by J.-Y. Huang *et al.* [55], demonstrating Stark tuning of single Er^{3+} in YSO using similar techniques.

*Present address: QphoX B.V., 2628XG Delft, The Netherlands.
†Present address: MESA+ Institute for Nanotechnology, University of Twente, 7500AE Enschede, The Netherlands.
‡s.groeblacher@tudelft.nl
§wolfgang.tittel@unige.ch

[1] H. J. Kimble, The quantum internet, Nature (London) **453**, 1023 (2008).
[2] S. Wehner, D. Elkouss, and R. Hanson, Quantum internet: A vision for the road ahead, Science **362**, eaam9288 (2018).
[3] N. Sangouard, C. Simon, H. de Riedmatten, and N. Gisin, Quantum repeaters based on atomic ensembles and linear optics, Rev. Mod. Phys. **83**, 33 (2011).
[4] A. Reiserer and G. Rempe, Cavity-based quantum networks with single atoms and optical photons, Rev. Mod. Phys. **87**, 1379 (2015).
[5] L.-M. Duan and C. Monroe, Colloquium: Quantum networks with trapped ions, Rev. Mod. Phys. **82**, 1209 (2010).
[6] P. Lodahl, Quantum-dot based photonic quantum networks, Quantum Sci. Technol. **3**, 013001 (2017).
[7] D. D. Awschalom, R. Hanson, J. Wrachtrup, and B. B. Zhou, Quantum technologies with optically interfaced solid-state spins, Nat. Photonics **12**, 516 (2018).
[8] M. Ruf, N. H. Wan, H. Choi, D. Englund, and R. Hanson, Quantum networks based on color centers in diamond, J. Appl. Phys. **130**, 070901 (2021).
[9] M. Pompili, S. L. N. Hermans, S. Baier, H. K. C. Beukers, P. C. Humphreys, R. N. Schouten, R. F. L. Vermeulen, M. J. Tiggelman, L. d. S. Martins, B. Dirkse, S. Wehner, and R. Hanson, Realization of a multinode quantum network of remote solid-state qubits, Science **372**, 259 (2021).
[10] S. L. N. Hermans, M. Pompili, H. K. C. Beukers, S. Baier, J. Borregaard, and R. Hanson, Qubit teleportation between non-neighbouring nodes in a quantum network, Nature (London) **605**, 663 (2022).
[11] M. K. Bhaskar, R. Riedinger, B. Machielse, D. S. Levonian, C. T. Nguyen, E. N. Knall, H. Park, D. Englund, M. Lončar, D. D. Sukachev, and M. D. Lukin, Experimental demonstration of memory-enhanced quantum communication, Nature (London) **580**, 60 (2020).
[12] B. Hensen, H. Bernien, A. E. Dréau, A. Reiserer, N. Kalb, M. S. Blok, J. Ruitenberg, R. F. L. Vermeulen, R. N. Schouten, C. Abellán, W. Amaya, V. Pruneri,

M. W. Mitchell, M. Markham, D. J. Twitchen, D. Elkouss, S. Wehner, T. H. Taminiau, and R. Hanson, Loophole-free Bell inequality violation using electron spins separated by 1.3 kilometres, Nature (London) **526,** 682 (2015).

[13] M. F. Askarani, A. Das, J. H. Davidson, G. C. Amaral, N. Sinclair, J. A. Slater, S. Marzban, C. W. Thiel, R. L. Cone, D. Oblak, and W. Tittel, Long-lived solid-state optical memory for high-rate quantum repeaters, Phys. Rev. Lett. **127,** 220502 (2021).

[14] C. W. Thiel, T. Böttger, and R. L. Cone, Rare-earth-doped materials for applications in quantum information storage and signal processing, J. Lumin. **131,** 353 (2011).

[15] A. I. Lvovsky, B. C. Sanders, and W. Tittel, Optical quantum memory, Nat. Photonics **3,** 706 (2009).

[16] M. P. Hedges, J. J. Longdell, Y. Li, and M. J. Sellars, Efficient quantum memory for light, Nature (London) **465,** 1052 (2010).

[17] M. Sabooni, Q. Li, S. Kröll, and L. Rippe, Efficient quantum memory using a weakly absorbing sample, Phys. Rev. Lett. **110,** 133604 (2013).

[18] J. H. Davidson, P. Lefebvre, J. Zhang, D. Oblak, and W. Tittel, Improved light-matter interaction for storage of quantum states of light in a thulium-doped crystal cavity, Phys. Rev. A **101,** 042333 (2020).

[19] A. Ortu, A. Holzäpfel, J. Etesse, and M. Afzelius, Storage of photonic time-bin qubits for up to 20 ms in a rare-earth doped crystal, npj Quantum Inf. **8,** 29 (2022).

[20] Y. Ma, Y.-Z. Ma, Z.-Q. Zhou, C.-F. Li, and G.-C. Guo, One-hour coherent optical storage in an atomic frequency comb memory, Nat. Commun. **12,** 2381 (2021).

[21] E. Saglamyurek, N. Sinclair, J. Jin, J. A. Slater, D. Oblak, F. Bussières, M. George, R. Ricken, W. Sohler, and W. Tittel, Broadband waveguide quantum memory for entangled photons, Nature (London) **469,** 512 (2011).

[22] Z.-Q. Zhou, W.-B. Lin, M. Yang, C.-F. Li, and G.-C. Guo, Realization of reliable solid-state quantum memory for photonic polarization qubit, Phys. Rev. Lett. **108,** 190505 (2012).

[23] T.-S. Yang, Z.-Q. Zhou, Y.-L. Hua, X. Liu, Z.-F. Li, P.-Y. Li, Y. Ma, C. Liu, P.-J. Liang, X. Li, Y.-X. Xiao, J. Hu, C.-F. Li, and G.-C. Guo, Multiplexed storage and real-time manipulation based on a multiple degree-of-freedom quantum memory, Nat. Commun. **9,** 3407 (2018).

[24] R. Kolesov, K. Xia, R. Reuter, R. Stöhr, A. Zappe, J. Meijer, P. Hemmer, and J. Wrachtrup, Optical detection of a single rare-earth ion in a crystal, Nat. Commun. **3,** 1029 (2012).

[25] A. M. Dibos, M. Raha, C. M. Phenicie, and J. D. Thompson, Atomic source of single photons in the telecom band, Phys. Rev. Lett. **120,** 243601 (2018).

[26] T. Zhong, J. M. Kindem, J. G. Bartholomew, J. Rochman, I. Craiciu, V. Verma, S. W. Nam, F. Marsili, M. D. Shaw, A. D. Beyer, and A. Faraon, Optically addressing single rare-earth ions in a nanophotonic cavity, Phys. Rev. Lett. **121,** 183603 (2018).

[27] J. M. Kindem, A. Ruskuc, J. G. Bartholomew, J. Rochman, Y. Q. Huan, and A. Faraon, Control and single-shot readout of an ion embedded in a nanophotonic cavity, Nature (London) **580,** 201 (2020).

[28] M. Raha, S. Chen, C. M. Phenicie, S. Ourari, A. M. Dibos, and J. D. Thompson, Optical quantum nondemolition

measurement of a single rare earth ion qubit, Nat. Commun. **11,** 1605 (2020).

[29] L. Yang, S. Wang, M. Shen, J. Xie, and H. X. Tang, Controlling single rare earth ion emission in an electro-optical nanocavity, Nat. Commun. **14,** 1718 (2023).

[30] A. Gritsch, A. Ulanowski, and A. Reiserer, Purcell enhancement of single photon emitters in silicon, Optica **10,** 783 (2023).

[31] S. Ourari, Ł. Dusanowski, S. P. Horvath, M. T. Uysal, C. M. Phenicie, P. Stevenson, M. Raha, S. Chen, R. J. Cava, N. P. de Leon, and J. D. Thompson, Indistinguishable telecom band photons from a single erbium ion in the solid state, Nature (London) **620,** 977 (2023).

[32] C. Deshmukh, E. Beattie, B. Casabone, S. Grandi, D. Serrano, A. Ferrier, P. Goldner, D. Hunger, and H. de Riedmatten, Detection of single ions in a nanoparticle coupled to a fiber cavity, arXiv:2303.00017.

[33] A. Kinos, D. Hunger, R. Kolesov, K. Mølmer, H. de Riedmatten, P. Goldner, A. Tallaire, L. Morvan, P. Berger, S. Welinski, K. Karrai, L. Rippe, S. Kröll, and A. Walther, Roadmap for rare-earth quantum computing, arXiv:2103.15743.

[34] M. Zhong, M. P. Hedges, R. L. Ahlefeldt, J. G. Bartholomew, S. E. Beavan, S. M. Wittig, J. J. Longdell, and M. J. Sellars, Optically addressable nuclear spins in a solid with a six-hour coherence time, Nature (London) **517,** 177 (2015).

[35] A. Ruskuc, C.-J. Wu, J. Rochman, J. Choi, and A. Faraon, Nuclear spin-wave quantum register for a solid-state qubit, Nature (London) **602,** 408 (2022).

[36] M. T. Uysal, M. Raha, S. Chen, C. M. Phenicie, S. Ourari, M. Wang, C. G. Van de Walle, V. V. Dobrovitski, and J. D. Thompson, Coherent control of a nuclear spin via interactions with a rare-earth ion in the solid-state, PRX Quantum **4,** 010323 (2023).

[37] S. D. Barrett and P. Kok, Efficient high-fidelity quantum computation using matter qubits and linear optics, Phys. Rev. A **71,** 060310(R) (2005).

[38] T.-M. Zhao, H. Zhang, J. Yang, Z.-R. Sang, X. Jiang, X.-H. Bao, and J.-W. Pan, Entangling different-color photons via time-resolved measurement and active feed forward, Phys. Rev. Lett. **112,** 103602 (2014).

[39] C. Gerry and P. Knight, *Introductory Quantum Optics* (Cambridge University Press, Cambridge, England, 2004).

[40] J. H. Prechtel, A. V. Kuhlmann, J. Houel, L. Greuter, A. Ludwig, D. Reuter, A. D. Wieck, and R. J. Warburton, Frequency-stabilized source of single photons from a solid-state qubit, Phys. Rev. X **3,** 041006 (2013).

[41] J. Guo and S. Gröblacher, Integrated optical-readout of a high-Q mechanical out-of-plane mode, Light Sci. Appl. **11,** 282 (2022).

[42] A. A. Kaplyanskii, Linear Stark effect in spectroscopy and luminescence of doped inorganic insulating crystals, J. Lumin. **100,** 21 (2002).

[43] S. R. Hastings-Simon, M. U. Staudt, M. Afzelius, P. Baldi, D. Jaccard, W. Tittel, and N. Gisin, Controlled Stark shifts in Er^{3+}-doped crystalline and amorphous waveguides for quantum state storage, Opt. Commun. **266,** 716 (2006).

[44] D. L. McAuslan, J. J. Longdell, and M. J. Sellars, Strong-coupling cavity QED using rare-earth-metal-ion dopants in monolithic resonators: What you can do with a weak oscillator, Phys. Rev. A **80**, 062307 (2009).

[45] See Supplemental Material at http://link.aps.org/supplemental/10.1103/PhysRevLett.131.170801, which includes Refs. [31,40,41,46–53], for details about the device design and fabrication, experimental setups as well as extended analysis and discussion of the ensemble and single-ion spectroscopy study.

[46] C. Thiel, R. Macfarlane, T. Böttger, Y. Sun, R. Cone, and W. Babbitt, Optical decoherence and persistent spectral hole burning in Er^{3+} : $LiNbO_3$, J. Lumin. **130**, 1603 (2010).

[47] A. Kaplyanskii and R. Macfarlane, *Spectroscopy of Solids Containing Rare Earth Ions*, Modern Problems in Condensed Matter Sciences (North-Holland, Amsterdam, 1987).

[48] R. M. Macfarlane, High-resolution laser spectroscopy of rare-earth doped insulators: A personal perspective, J. Lumin. **100**, 1 (2002).

[49] S. Wang, L. Yang, M. Shen, W. Fu, Y. Xu, R. L. Cone, C. W. Thiel, and H. X. Tang, Er : $LiNbO_3$ with High optical coherence enabling optical thickness control, Phys. Rev. Appl. **18**, 014069 (2022).

[50] C.-H. Huang, L. McCaughan, and D. M. Gill, Evaluation of absorption and emission cross sections of Er-doped $LiNbO_3$ for application to integrated optic amplifiers, J. Lightwave Technol. **12**, 803 (1994).

[51] M. F. Askarani, Marcel Li Grimau Puigibert, T. Lutz, V. B. Verma, M. D. Shaw, S. W. Nam, N. Sinclair, D. Oblak, and W. Tittel, Storage and reemission of heralded telecommunication-wavelength photons using a crystal waveguide, Phys. Rev. Appl. **11**, 054056 (2019).

[52] V. S. Lethokov, *High-Resolution Laser Spectroscopy*, Topics in Applied Physics (Springer, Berlin, 1976).

[53] A. Reiserer, Colloquium: Cavity-enhanced quantum network nodes, Rev. Mod. Phys. **94**, 041003 (2022).

[54] T. Zhong, J. M. Kindem, J. G. Bartholomew, J. Rochman, I. Craiciu, E. Miyazono, M. Bettinelli, E. Cavalli, V. Verma, S. W. Nam, F. Marsili, M. D. Shaw, A. D. Beyer, and A. Faraon, Nanophotonic rare-earth quantum memory with optically controlled retrieval, Science **357**, 1392 (2017).

[55] J.-Y. Huang, P.-J. Liang, L. Zheng, P.-Y. Li, Y.-Z. Ma, D.-C. Liu, J.-H. Xie, Z.-Q. Zhou, C.-F. Li, and G.-C. Guo, Stark tuning of telecom single-photon emitters based on a single Er^{3+}, Chin. Phys. Lett. **40**, 070301 (2023).